ELSEVIER

Journal of Molecular Catalysis A: Chemical 163 (2000) 67–77

JOURNAL OF MOLECULAR CATALYSIS A: CHEMICAL

www.elsevier.com/locate/molcata

Surface catalytic reactions assisted by gas phase molecules: activation of reaction intermediates

Takafumi Shido, Aritomo Yamaguchi, Kiyotaka Asakura[1], Yasuhiro Iwasawa*

Department of Chemistry, Graduate School of Science, The University of Tokyo, Hongo, Bunkyo-ku, Tokyo 113-0033, Japan

Received 6 March 2000; accepted 20 March 2000

Abstract

This paper attempts to review our recent work to provide an aspect of catalysis "surface catalytic reactions assisted by gas phase molecules", describing the previous representative results and also presenting new data. In this concept, reaction intermediates are activated by gas phase molecules which adsorb weakly or are undetectable at the surface. The examples are the ethanol dehydrogenation on Nb/SiO_2, the water gas shift reactions on MgO, ZnO and Rh/CeO_2, and the NO–CO reaction on Co/Al_2O_3.

Keywords: Catalytic reaction mechanism; Catalysis concept; FT-IR, EXAFS; Water gas shift reaction; Ethanol dehydrogenation; NO reduction; MgO; ZnO; Rh.CeO; Nb/SiO_2; Co/Al_2O_3; Co/TiO_2; Co/SiO_2

1. Introduction

While it has been recognized that control and activation of reaction intermediates are critical in achieving selective performance of catalysts, this issue has not been adequately addressed and is a serious challenge to the field.

The aim of this paper is to illustrate how weakly adsorbed molecules or undetectable molecules at the surface can promote surface catalytic reactions. Weakly adsorbed molecules at catalyst surfaces can exist only under catalytic reactions conditions in the presence of gas phase molecules. Recently we have found that weakly adsorbed molecules can activate the reaction of strongly-adsorbed intermediates, ultimately controlling the catalytic reaction path [1,2]. We have also discovered a surface event that gas phase molecules undetectable at the surface can change the structure, amount and reactivity of intermediates [3–5]. In this paper three typical examples of reactions are presented, i.e. the water gas shift reaction on basic metal oxide catalysts with and without supported metals, the ethanol dehydrogenation on designed Nb monomers supported on SiO_2, and the NO–CO reaction on designed Co monomers and ensembles supported on Al_2O_3, TiO_2 and SiO_2.

Reaction intermediates at catalyst surfaces are often unstable and not naturally observed by spectroscopic methods. To elucidate the key issues to activate the intermediates and to control its reactivity (selectivity of the reaction), it is preferable that the reaction intermediates are stable enough to be detectable spectroscopically under the working conditions. The intermediates, formate, ethoxy, and dinitrosyl species, respectively in the above three catalytic reactions are observable under the reaction conditions by FT-IR.

* Corresponding author. Fax: +81-3-5800-6892.
E-mail address: iwasawa@chem.s.u-tokyo.ac.jp (Y. Iwasawa).
[1] Present address: Catalysis Research Center, Hokkaido University, Kita-ku, Sapporo 060-0811, Japan.

1381-1169/00/$ – see front matter
PII: S1381-1169(00)00400-3

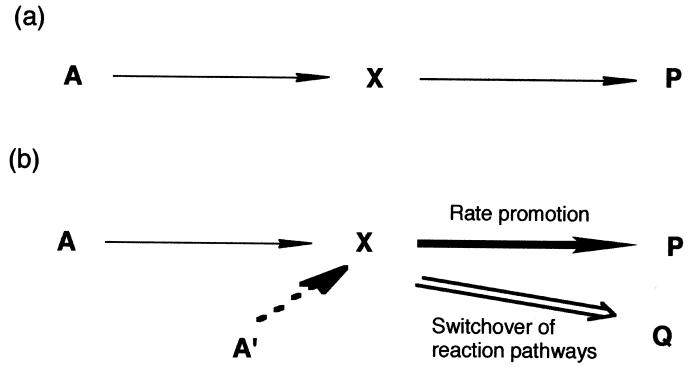

Fig. 1. Surface catalytic reactions assisted by gas phase molecules: Surface catalytic reaction (A → P) via intermediate X (b) Surface catalytic reaction (A → P) promoted by reactant molecule or coexisting molecules A′ in the gas phase, where enhancement of the reaction rate for the formation of P or switchover of the reaction path from P formation to Q formation is caused by A′.

2. Surface catalytic reactions assisted by gas phase molecules

A simplified form of the usual mechanism for heterogeneous catalytic reactions is shown in Fig. 1(a), where the reaction intermediate (X) is transformed to the product (P) by surface unimolecular decomposition; that is, a stoichiometric reaction step proceeds without aid of other molecules [2]. In a typical catalyst, a role of the active site is to directly activate the adsorbed intermediate, which makes it possible for the bond rearrangement to occur in a desired manner. A typical example is seen for ethanol oxidation on Mo-oxide catalysts, where Mo-ethoxide intermediate (Mo–OC_2H_5) (X) at the surface decomposes by itself to a product, acetaldehyde (P), and the behavior of the intermediate is similar under vacuum and catalytic reaction conditions when the surface coverage is identical under both atmospheres [6,7]. The feature would also be valid for the Langmuir–Hinshelwood mechanism for e.g. $CO + 1/2O_2 \rightarrow CO_2$, in which two adsorbed species (CO(a) and O(a)) independently interact with the surface sites and subsequently react with each other; $A + B \rightarrow X \rightarrow P$. The surface reaction requires no additional gas phase molecules.

In contrast to the simple expectation of no special role of additional gas phase molecules in a catalytic mechanism, we have found evidence that the reaction intermediate of an important catalytic reaction can be profoundly influenced by the ambient gas. In particular, the reaction involved the SiO_2-supported niobium monomer catalyst which was the first to be active for dehydrogenation of ethanol, $C_2H_5OH \rightarrow CH_3CHO + H_2$ [8]. Niobium has attracted much attention as a key element for industrially important processes such as ammoxidation of propane [9], oxidative dehydrogenation of propane [10], and liquid-phase catalysis [11]. In the catalytic dehydrogenation reaction of ethanol on the Nb/SiO_2 catalyst the intermediate (X) was stable and did not decompose to a product (P) upto 600 K, whereas in the coexistence of another reactant molecule (A′) the intermediate (X) is activated to decompose to a different product (Q) even at low temperatures like 473 K (Fig. 1(b)) [12]. Enhancement of the rate of the intermediate decomposition and switchover of the reaction path in Fig. 1(b) were also found in water gas shift reactions on MgO, ZnO and Rh/CeO_2 [13–17]. Change in structure, amount and reactivity of the intermediate was also found in NO–CO reaction on Co/Al_2O_3 [3–5]. These three reactions are described below.

3. Switchover of the reaction paths in the ethanol dehydrogenation on Nb/SiO_2

The SiO_2-supported Nb catalyst (**1**) exhibits high activity and selectivity for the dehydrogenation reaction. Acetaldehyde and hydrogen were stoichiometrically produced during the catalytic reaction as shown in Fig. 2 [12]. Ethanol dissociatively adsorbs on Nb to form C_2H_5O(a) and OH(a) in Scheme 1

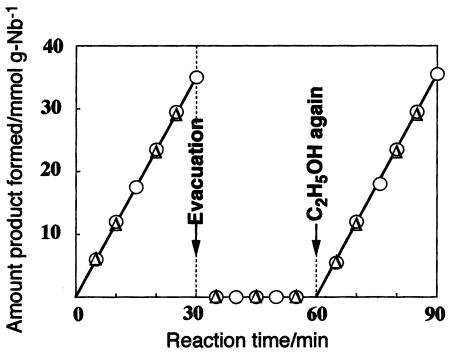

Fig. 2. Ethanol dehydrogenation on Nb/SiO_2 (○: H_2, △: CH_3CHO).

[2,4]. This is proved by IR spectra using C_2H_5OH, C_2H_5OD and C_2D_5OH [12]. The adsorbed species OH(a) and C_2H_5O(a) are stable in vacuum, while the exchange reaction with the gas phase ethanol readily occurs [12]. The ν(OH) peak and the ν(CH) peaks are only observed peaks under the catalytic C_2H_5OH dehydrogenation reaction conditions.

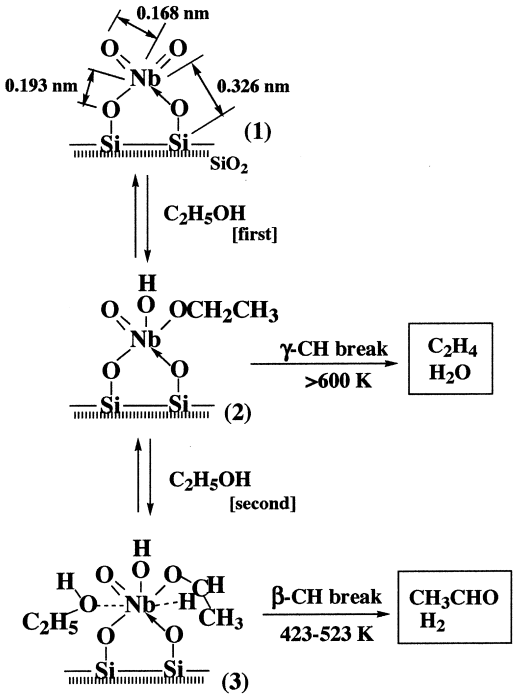

Scheme 1. Switchover of the reaction paths by weak ethanol coordination.

When the gas-phase ethanol was evacuated in the course of the dehydrogenation at 523 K, the reaction completely stopped as shown in Fig. 2. However, the amount of adsorbed ethanol (Species (**2**) in Scheme 1), remained unchanged by the evacuation as evidenced by the intensity of the ν(OH) and ν(CH) peaks. In other words, the adsorbed ethanol was converted selectively to acetaldehyde and hydrogen under the ambient ethanol at 423–523 K, whereas the adsorbed ethanol was never decomposed under vacuum in the same temperature range. This might be a strange aspect in a sense because the ethanol dehydrogenation has been thought to be a surface reaction which proceeds via decomposition of the adsorbed ethanol and which rate depends only on the coverage of the adsorbed ethanol, not on the pressure of gas phase molecules. To gain insight into the reactivity of adsorbed ethanol, a temperature programmed desorption (TPD) spectrum for the Species (**2**) formed during the catalytic ethanol dehydrogenation reaction was measured as shown in Fig. 3, which revealed that the reaction of adsorbed ethanol (**2**) in vacuum was only possible at higher temperatures than 600 K, with a TPD peak at 700 K. The TPD peak is observed in the much higher temperature range than 423–523 K for the catalytic reactions, and the TPD products are ethene and water (dehydrated products), contrasted to acetaldehyde and hydrogen (dehydrogenated products) produced in the catalytic reactions. The dehydrogenation reac-

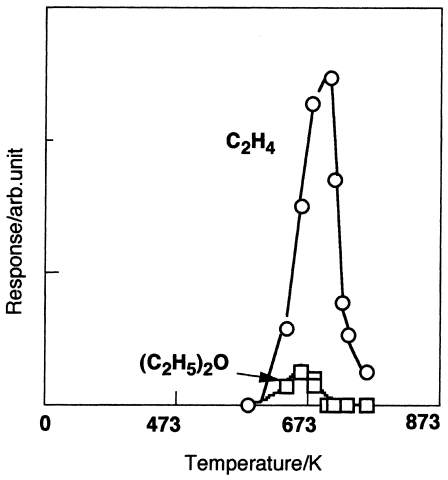

Fig. 3. TPD spectrum from species (**2**).

tion started again by introducing ethanol vapor onto Species (**2**) as shown in Fig. 2. Thus, it seems that the catalytic dehydrogenation reaction is assisted by the ambient ethanol, where the reaction path of adsorbed ethanol (**2**) is switched from dehydration to dehydrogenation by the ambient ethanol. In other words, Species (**2**) prefers the dehydration to form ethene and water by *the γ-hydrogen abstraction*, while in the presence of the ambient ethanol *the β-hydrogen abstraction* from Species (**2**) to form acetaldehyde and hydrogen dominates as shown in Scheme 1.

To examine how and why the surface ethanol reaction is assisted by the gas-phase ethanol, the following experiments were conducted in a closed circulating reactor. Ethanol vapor was first admitted onto the dioxo-Nb monomer catalyst (**1**) to form Species (**2**) at 373 K, followed by evacuation, and then the system was maintained at 523 K for 10 min, where no H_2 evolution was observed because the Species (**2**) was stable up to 600 K in vacuum. After the confirmation of neither H_2 nor CH_3CHO formations, various electron-donating compounds were post-adsorbed on the Species (**2**) at 523 K, which led to a stoichiometric evolution of H_2 and CH_3CHO. Logarithm of the initial rates of the $CH_3CHO(H_2)$ formation from the pre-adsorbed ethanol (**2**) was plotted against donor number of the post-adsorbed molecules which undissociatively adsorb on the Nb atom, where the donor number is regarded as electron-donor strength of the post-adsorbed molecules [2,12]. Linear relationship observed between them indicates that the electron donor–acceptor interaction between the post-adsorbed molecule and the coordinatively unsaturated Nb d^0 ion is a key issue for the dehydrogenation of the pre-adsorbed ethanol (**2**) [12].

Thus the catalytic dehydrogenation reaction of ethanol is likely to proceed via Species (**3**) involving a second (post-adsorbed) ethanol molecule as shown in Scheme 1. The weakly adsorbed ethanol (post-adsorbed) (**3**) present only under the catalytic reaction conditions in Scheme 1 was kinetically characterized [12]. Further, all the kinetic data well fit the mechanism of Scheme 1. The dehydrogenation mechanism in Scheme 1 reveals the switchover of the reaction path from dehydration (γ-CH bond break) to dehydrogenation (β-CH bond break) by whether or not ethanol molecules are present in the gas phase. Even if adsorbed species at surface is too stable in vacuum, the catalytic reaction is possible to proceed through the same species by assist of a second reactant molecule (reactant-promoted mechanism) [8,12].

4. Activation of the reaction intermediates in water gas shift reactions on MgO, ZnO and Rh/CeO_2

The water gas shift (WGS) reaction ($H_2O + CO = H_2 + CO_2$) on MgO, ZnO and Rh/CeO_2 is another example of a surface catalytic reaction that is assisted by gas phase molecules [18]. The behavior of surface formate intermediates ($HCOO^-$) is remarkably influenced by weakly coadsorbed water molecules that can exist only under the ambient water [1,2,13–17]. Water dissociatively adsorbs to form OH groups on many oxide surfaces. The formate is produced from the OH groups and CO. The local structure of OH groups have been characterized in detail by FT-IR. The structure of the formates, unidentate, bidentate, and bridge types, can also be determined by the value of $\Delta\nu = \nu_{as}(OCO) - \nu_s(OCO)$ [19]. When $\Delta\nu$ is larger or smaller than that of a free ion, the formate is considered to be unidentate or bidentate, respectively. When it is as large as that of a free ion, it is assigned to be of bridge type. Discrimination of three different formates on the oxide surfaces is possible when at least two types of formates are observed on those surfaces. These surface formates are detectable under the working conditions by FT-IR. Thus the WGS reaction may be another good system to study the origin of the genesis for catalysis on a molecular level.

On MgO unidentate formate was produced at low temperatures, and then bidentate (minor) and bridge (major) formates were produced with increasing temperature. The unidentate formate was preferably transformed to the bridge formate in the presence of water vapor. Thus the bridge formate was main species under the catalytic WGS reaction conditions on MgO [13].

It was found that the bridge formate produced from OH group (H_2O) and CO was never converted to the products, H_2 and CO_2, in vacuum, whereas the formate has been positioned as reaction intermediate for the catalytic WGS reaction [13]. To clarify the reason of the difference in behavior of the surface formate under vacuum and in the working state, decomposition of the surface formate was examined. Table 1 shows

Table 1
The rate constants, k_+ and k_-, of the forward and backward decompositions of the D-labeled formates (COO^-) in vacuum and under the ambient D_2O[a]

Catalyst	Reaction temperature. (*K*)	Gas phase	$k_+ + k_-$ (s^{-1})	k_+/k_-	Ea (k_+) ($kJ\,mol^{-1}$)
MgO	600	vacuum	1.3×10^{-4}	0/100	–
		D_2O	1.9×10^{-4}	74/26	–
ZnO	533	vacuum	1.3×10^{-4}	26/74	155
		D_2O	5.3×10^{-4}	100/0	109
Rh/CeO_2	443	vacuum	1.1×10^{-5}	35/65	56
		D_2O	1.1×10^{-3}	100/0	33

[a] 0.40 kPa for ZnO and 0.67 kPa for MgO and Rh/CeO_2, and the activation energies for the forward reactions.

the rate constants, k_+ and k_-, for the *forward* decomposition of the surface formate to form $H_2 + CO_2$ and *backward* decomposition of the surface formate to form $H_2O + CO$, respectively, without and with water vapor (0.67 kPa).

$$H_2O + CO \overset{\text{backward decomposition}}{\leftharpoondown} HCOO^-(a)$$
$$+H^+(a) \overset{\text{forward decomposition}}{\rightharpoonup} H_2 + CO_2$$

Note that k_+ for the forward decomposition of the formate to produce $H_2 + CO_2$ was zero in vacuum, whereas in the presence of gas-phase water the formation of H_2 and CO_2 was observed. The backward decomposition of the formate to $H_2O + CO$ was markedly suppressed and the forward decomposition path was opened, by coexistence of water vapor. Change of the selectivity of the formate decomposition is not due to a thermodynamical shift because the total quantity of OH groups and adsorbed water increased only two-three times by the presence of gas-phase water compared to that in vacuum, while a drastic change in selectivity occured by the ambient water as shown in Table 1. Rather, the decomposition is kinetically controlled, where gas-phase water molecules induce the dehydrogenation path of the surface formate to form CO_2 and H_2.

The surface formate was stabilized by coadsorbed water as revealed by upshift of the TPD peak, suggesting interaction of the formate with the coadsorbed water. It was demonstrated that the electron-donating and withdrawing interaction of water molecule with the Mg–O pair site is a key issue for the forward decomposition of the bridge formate to produce H_2 and CO_2 [13]. At the reaction temperature like 600 K the coadsorbed water molecules can exist only under the ambient water, and hence the surface reaction is successively assisted by the gas phase molecule.

It has been demonstrated from FT-IR and kinetic data that the catalytic WGS reaction on ZnO proceeds as follows [14]. The first water molecule dissociates at mainly Zn_{2c}–O_{3c} pair to form a linear OH group and a bridge or threefold-hollow OH group. The linear OH group on Zn reacts with CO to produce the bidentate formate through unidentate formate. Seventy percents of the formates backwardly decompose to the original H_2O and CO under vacuum and only 30% of them forwardly decompose to react with the bridge or threefold hollow OH groups to produce H_2 and CO_2. In the presence of gas phase water, the weakly adsorbed (second) water molecule adsorbs on the Zn atom and enhances the forward decomposition, where almost 100% of the formates decompose to H_2 and CO_2 [14].

It was found that the rate constant of the forward decomposition of the surface bidentate formate ($DCOO^-$) to produce D_2 and CO_2 increased from 0.34×10^{-4} under vacuum to $5.3 \times 10^{-4}\,s^{-1}$ under the ambient water. Electron donors such as NH_3, CH_3OH, pyridine and THF also increased the decomposition rate. It is likely that one of the driving force for the forward decomposition of the formate is electron donation of the adsorbed molecule to the Zn ion on which the bidentate formate adsorbs. The reactant-promoted mechanism for the catalytic WGS reaction on ZnO is illustrated in Scheme 2. The activation energy for the forward decomposition of the formate decreases from 155 under vacuum to $109\,kJ\,mol^{-1}$ under the ambient water as shown in Table 1 [14].

The WGS reaction is a reversible reaction, that is, WGS reaction attains equilibrium with reverse WGS reaction. Thus the fact that the WGS reaction is

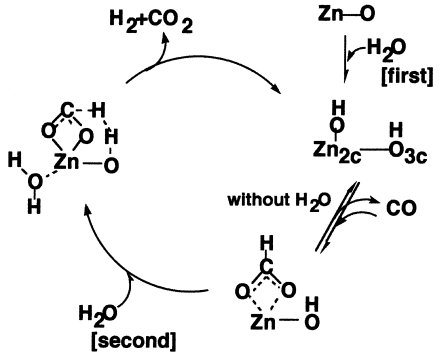

Scheme 2. Water gas shift reaction promoted by weakly adsorbed water on ZnO.

promoted by H_2O (a reactant), in turn, implies that the reverse WGS reaction may also be promoted by a reactant, H_2 or CO_2. In fact the decomposition of the surface formates produced from $H_2 + CO_2$ was promoted 8–10 times by gas-phase hydrogen [16]. Change in the selectivities for the decomposition of the formates produced from $H_2O + CO$ and for the decomposition of the formates produced from $H_2 + CO_2$ is shown as follows.

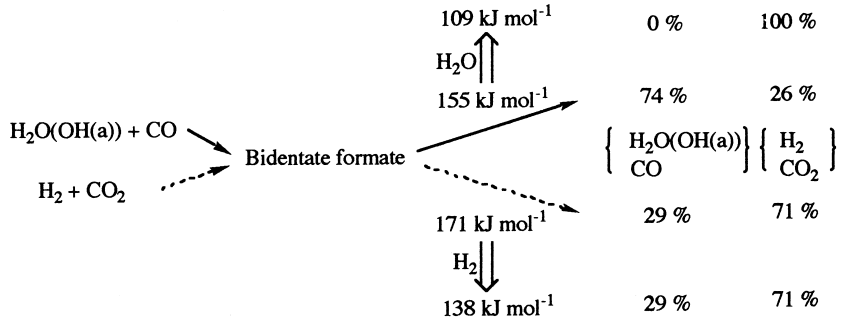

The drastic difference in selectivity should not be ascribed to the difference of the bonding feature in the Zn-formate species because of almost the same frequencies of ν(CH), ν_{as}(OCO) and ν_s(OCO) for both bidentate formates produced from H_2O+CO and H_2+CO_2. Note that the origin ($H_2O + CO$ or $H_2 + CO_2$) from which the formate is produced is 'remembered' as a main decomposition path under vacuum, while the origin is "forgotten" by coadsorbed H_2O. The WGS and reverse WGS reactions conceivably proceed on different formate sites of the ZnO surface unlike usual catalytic reaction kinetics, while the occurrence of the reactant-promoted reactions does not violate the principle of microscopic reversibility [2].

In the reverse WGS reaction hydrogen promoted both decomposition paths of the formate to $H_2 + CO_2$ and $H_2O + CO$, and the decomposition selectivity did not change. Thus, the mechanism of promotion of hydrogen is different from that of electron donors in the WGS reaction. CO_2 not only blocked the adsorption sites of H_2 but also suppressed the decomposition of the formate intermediate.

Rh catalysts with CeO_2 have been used as automobile exhaust catalysts [20], on which WGS reaction proceeds. In the catalytic WGS reaction on Rh/CeO_2, linear OH groups reacted with CO to produce the bidentate formates. In vacuum, 65% of the surface formates decomposed backwardly to H_2O+CO and 35% of them decomposed forwardly to $H_2 + CO_2$. When water vapor coexisted, 100% of the formates decomposed forwardly to H_2+CO_2 as shown in Table 1. The activation energy for the forward decomposition of the formate decreased from 56 in vacuum to 33 kJ mol^{-1} by the presence of water vapor. The value of the forward decomposition rate constant (k_+) was promoted about 100 times by coexistence of gas phase water [17].

The isotope effect was observed with the hydrogen atom of the formate and not observed with the hydrogen atom of water molecule. The result is similar to that observed on ZnO, where the rate-determining step of the formate decomposition is suggested to be dissociation of the CH bond of the bidentate formate. In summary, the reaction mechanism for the catalytic WGS reaction on Rh/CeO_2 is essentially the same as that on ZnO.

5. Surface atalytic NO–CO reaction promoted by undetectable CO on Co/Al_2O_3

A Co/Al_2O_3 catalyst (**4**) was prepared in a similar manner to that reported in the literature [21,22]; $Co_2(CO)_8$ was supported on Al_2O_3 (Degussa Alon C) by a chemical vapor deposition method, to form $Co_4(CO)_8/Al_2O_3$, followed by the two controllable steps, $Co_4(CO)_{12}/Al_2O_3 \rightarrow [CoO]_4/Al_2O_3 \rightarrow [Co^{2+}]_4/Al_2O_3$ (**4**).

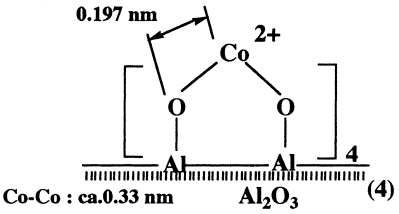

The activity of the Co/A_2O_3 catalyst (**4**) for NO–CO reaction was much higher than that of a conventional impregnation Co/Al_2O_3 catalyst [4,5]. The products of the catalytic NO–CO reaction in the temperature range 353–463 K were N_2O and CO_2. In the more elevated temperatures N_2O was further converted to N_2, where N_2 and CO_2 were main products by the equations $2NO+CO \rightarrow N_2O+CO_2$ and $N_2O+CO \rightarrow N_2 + CO_2$.

In this article the first reaction step, $2NO + CO \rightarrow N_2O + CO_2$, has been studied from the mechanistic interest.

Fig. 4 depicts TPD spectra after NO adsorption of different periods on Co/Al_2O_3 in the absence of gas phase CO showed NO desorption simply, where little N_2O product was observed [5]. The higher temperature peak around 450 K became larger with increasing NO adsorption period. On the other hand, almost all of adsorbed NO molecules were evolved as N_2O in the presence of gas phase CO above 325 K. The TPD demonstrate that adsorbed NO is not transformed by the two-stage redox mechanism, $2NO \rightarrow N_2O+O(a)$ (rate-determining), $O(a)+CO \rightarrow CO_2$ (rapid), which has been proposed in many catalytic systems. The TPD data also reveal that the reactivity of adsorbed NO is remarkably promoted by gas phase CO molecules. Note that CO molecules which promote the surface NO conversion were volumetically and spectroscopically undetectable as adsorbates on the Co/Al_2O_3 catalyst surface [3,4].

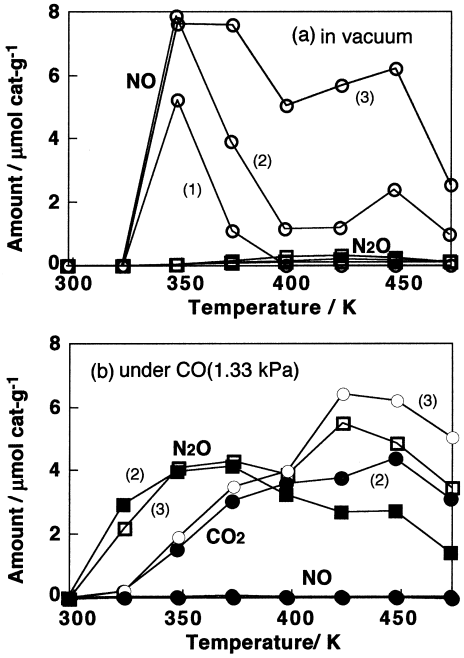

Fig. 4. TPD spectra in vacuum and under CO (1.33 kPa), following (1) NO (1.41 kPa) adsorption for 3 min and evacuation for 5 min, (2) NO (1.41 kPa) adsorption for 30 min and evacuation for 5 min, (3) NO (1.41 kPa) adsorption for 5 h and evacuration for 5 min; heating rate: 3.1 K/min; Co/Al_2O_3: 0.505 g; Co: 2.2 wt.%.

As the adsorbed state of NO seemed to change during the adsorption, the behavior of adsorbed NO species was monitored by in-situ FT-IR and XAFS. NO molecules adsorb as dinitrosyls on a Co atom $Co(NO)_2$ [4]. The bond angle(θ) between the two NO ligands on a Co atom (angle: NO–Co–NO) has been demonstrated to be related to the ratio of the antisymmetric stretching peak intensity (I_{as}) to the symmetric stretching peak intensity (I_s) for the dinitrosyl groups by the equation, $I_{as}/I_s = \tan 2(\theta/2)$ [23]. The amount of adsorbed NO (n_{NO}) is also estimated by the equation, $n_{NO} = \alpha I_{as}/\sin^2(\theta/2)$ (α is constant). The calculated θ and n_{NO} of the dinitrosyls on Co/Al_2O_3 are plotted against exposure time and evacuation time in Fig. 5 [5]. The change in n_{NO} completely coincided with the change in the amount of adsorbed NO determined gravimetrically in a quartz micro-balance in a separate experiment. Fig. 5 reveals that there are two kinds of dinitrosyls (species A and B) the dinitrosyl with a small bond angle (species A) is rapidly

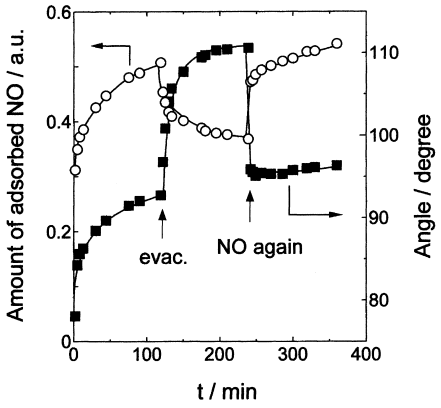

Fig. 5. The amount of adsorbed NO and the bond angle of $Co(NO)_2$ on Co/Al_2O_3 estimated from the FT-IR data (deconvoluted peak intensities) at room temperature. The previous values of the bond angle and amount of the $Co(NO)_2$ were estimated using the FT-IR peak intensities without deconvolution of the two peaks.

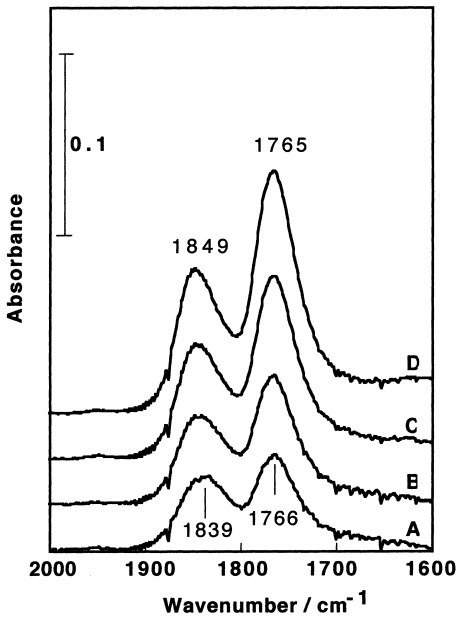

Fig. 6. FT-IR spectra for NO adsorbed on Co/Al_2O_3 at 463 K; NO = 1.33 kPa; CO (1.33 kPa) at 20 min after spectrum B; A: NO (5 min), B: NO (20 min), C: NO + CO (5 min), D: NO + CO (30 min).

formed upon NO adsorption and easily desorbed by evacuation at room temperature, while the dinitrosyl with a large bond angle (species B) is slowly formed and not desorbed by evacuation at room temperature. We estimate the ratio of species A to species B to be 1:2.1 at room temperature [4]. As the bond angle θ of species B was 111° and the θ for a mixture of species A and species B at 250 min of Fig. 5 was 96°, the θ for species A at room temperature was estimated to be 65°. Reintroduction of NO recovered the n_{NO} and the θ nearly to the original values before the evacuation.

Fig. 6 shows typical FT-IR spectra for NO adsorbed on the Co/Al_2O_3 catalyst at 463 K [5]. The intensities of the two peaks at 1839 (ν_s) and 1767 (ν_{as}) cm^{-1} increased by CO introduction, accompanied with increase in their relative ratio (I_{as}/I_s) (Fig. 6 C& D). These results demonstrate that the bond angle θ and the amount n_{NO} of adsorbed NO markedly increased under the ambient CO. The ν_s peak shifted from 1839 to 1849 cm^{-1} after the θ expansion, while the ν_{as} peak remained unchanged.

Fig. 7 shows the effects of CO on the bond angle and amount of adsorbed NO at 323, 373, 423, 448 and 463 K [4]. The amount of the dinitrosyls decreased with increasing temperature, while the bond angle θ increased with an increase of temperature. When CO was introduced to the system, the bond angle θ of the surface dinitrosyls increased. The degree of the angle expanding was different at temperatures and larger at higher temperatures, and at 323 K almost no effect was observed. It was also found that the amount of the dinitrosyls increased by CO admission. Again, the degree of the increase was larger at higher temperatures. At 463 K, the amount of the dinitrosyls was increased by the presence of the gas phase CO about twice as compared to the amount in the case of NO alone. The enhancement of the NO adsorption by the gas phase CO was not observed at 323 K. Thus, the effects of the ambient CO were large at the temperatures where the catalytic NO–CO reactions proceeded significantly, whereas the bond angle and amount of the dinitrosyls did not change by the presence of CO at 323 K, where the catalytic NO–CO reaction was negligible.

As CO is not observed at the surface, the conformation change to the spacious dinitrosyls and the increase of the amount of adsorbed NO might be collision-induced events. However, N_2 and Ar showed no effect on the adsorbed NO species at 463 K, which would exclude a possibility of the θ extension and the n_{NO} increase by a physical collision energy. Other explanation is necessary for the θ and the n_{NO} increase.

To shed light on the mechanism for the conformation change to the spacious dinitrosyls and the

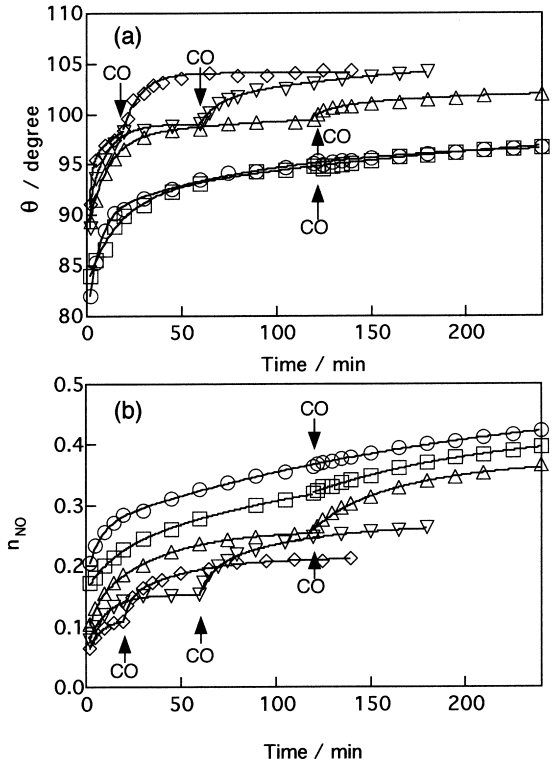

Fig. 7. Time profiles of and CO effects on the bond angles and amounts of the dinitrosyls on Co/Al_2O_3 (**4**); NO: 1.3 kPa, CO: 1.3 kPa; ○: 323 K; □: 373 K; △: 423 K; ▽: 448 K; ◇: 463 K.

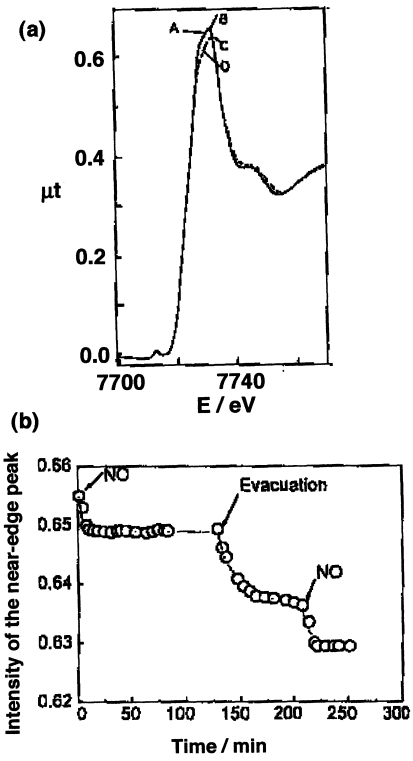

Fig. 8. Co K-edge XANES spectra for Co/Al_2O_3; A: fresh sample, B: after exposure to 1.3 kPa of NO at 463 K for 130 min, C: after evacuation at 463 K for 80 min after B, D: after re-exposure to 1.3 kPa of NO at 463 K for 50 min.

increase of the amount of adsorbed NO gas phase CO molecules undetectable at the surface, the local structure of the Co^{2+} species on Al_2O_3 was investigated by EXAFS. However, we were not able to find any change in the EXAFS data for the Co-dinitrosyls before and after CO introduction. Then we measured the Co K-edge XANES spectra for Co/Al_2O_3. The XANES spectra in Fig. 8(a) showed small but significant changes upon NO adsorption, evacuation and NO readsorption. The time-resolved profile of the change in the edge peak intensity is plotted in Fig. 8(b). When NO adsorbed on the catalyst, the edge peak decreased. The peak intensity was not recovered by NO evacuation, instead the larger decrease occurred as compared to the case of adsorption. The peak intensity decreased further by NO reintroduction. The results imply that an irreversible change on the Co sites occurred probably geometrically. This is contrasted to the reversible feature for the adsorbed NO species characterized by FT-IR in Fig. 5. Thus the XANES spectral change during NO adsorption and desorption may reflect the irreversible structure change at the interface between the Co^{2+} ions and the Al_2O_3 surface.

The observed surface catalytic NO–CO reactions assisted by gas phase CO molecules undetectable at the catalyst surface are summarized as follows. (1) The amount of adsorbed NO (Co-dinitrosyls) increased by the presence of gas phase CO. (2) The bond angle of the dinitrosyls increased by the presence of gas phase CO. (3) The reactivity of the dinitrosyls was promoted by the gas phase CO. The detection limit for CO adsorption is of the order of less than 5×10^{-3} CO per Co. If spectator CO molecules below the detection limit at the surface are assumed to play a role in the phenomena, one CO molecule must influence and activate more than 200 Co-dinitrosyls within the short residence period. We can not find the origin of this peculiar surface event, where undetectable CO with so

weak coordination to Co^{2+} ions remarkably modify the property of the Co^{2+} ions with the dinitrosyls. It may be possible to assume the presence of short-lived adsorbed CO molecules at the catalyst surface. The collision frequency for impinging CO on the Co^{2+} sites is roughly $5 \times 10^7\ s^{-1}$. If they stay at the surface for 10^{-10} s on average, the total residence-time of CO molecules at the surface corresponds to the amount of 5×10^{-3} Co in agreement with the detection limit for CO adsorption in the present study. This means that 99.5% of the Co^{2+} sites on average are always free without interaction with CO. Thus we propose an irreversible memory effect of a short lifetime CO species on the surface dinitrosyls. The irreversible effect may be supported by the fact that the high NO decomposition activity was maintained after evacuation during the course of the catalytic NO–CO reaction. This may also be related to the irreversible feature in the XANES data. The spectator CO molecules activate the $Co(NO)_2$ species, changing the structure from the small bond angle to the large bond angle during the total residence time. The spacious $Co(NO)_2$ induced by the impinging CO molecules under the catalytic reaction conditions may be more stable and reactive than the $Co(NO)_2$ with the narrow bond angle, which leads to the increase in the amount and reactivity of adsorbed NO at the reaction temperatures.

In contrast to the feature on the Co/Al_2O_3 catalyst, the θ and n_{NO} of Co-dinitrosyl species on Co/TiO_2 and Co/SiO_2 were little affected by the gas phase CO [5]. These catalysts have different structures around Co atoms [25]. The Co^{2+} ions in the Co/Al_2O_3 catalyst (**4**) are located as ensembles (probably four-Co ensembles; Co-Co: ca.0.33 nm) at the Al_2O_3 surface [24], whereas the Co^{2+} ions in the Co/TiO_2 and Co/SiO_2 catalysts are isolatedly distributed as monomers at the TiO_2 and SiO_2 surfaces, respectively. The amount of NO adsorbed on the Co^{2+} ions in the Co/Al_2O_3 catalyst was unity at saturation, while NO adsorbed as the dinitrosyls always. These results mean that half of the Co^{2+} ions are vacant with NO coordination under the catalytic reaction conditions. Thus a vacant Co^{2+} ion exists in vicinity of a Co^{2+} ion with adsorbed NO (dinitrosyl). We propose that CO molecules can adsorb on the vacant Co^{2+} ion at a short residence time even if the adsorbed amount is less than the detection limitation, in such a manner that the spectator CO molecule on a Co^{2+} ion has interaction to modify the structure of the Co-dinitrosyl on the adjacent Co^{2+} ion including a change in bonding feature at the surface interface as illustrated in Fig. 9. Further investigation is necessary for deeper understanding of the catalytic aspect on the Co/Al_2O_3 catalyst.

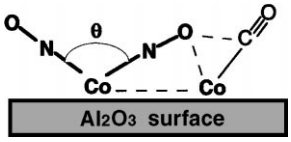

Fig. 9. A proposed picture for the effect of spectator CO on the conformation change and reactivity increase of the dinitrosyls.

6. Conclusion

As described above, weakly adsorbed molecules or impinging molecules under catalytic reaction conditions play an important role in surface catalytic reactions even if the adsorption of 'promotor' is very weak or is undetectable. Surface intermediates under the ambient gas behave in a different way from those under vacuum, showing rate enhancement and selectivity change of the surface reaction on the basis of the concept of surface catalytic reactions assisted by gas phase molecules. The concept suggests new strategies for development of catalytic materials and systems through in-situ activation of inactive and stable surface sites under the conditions of a target catalytic reaction.

Acknowledgements

The authors thank Dr. M. Nelson, Mr. S. Takahara, and Ms. A. Kameyama for their data acquisitions and helpful discussion. A part of this work has been supported by CREST (Core Research for Evolutional Science and Technology) of Japan Science and Technology Corporation (JST). The XAFS measurements have been done in the approval of Photon Factory advisory committee (Proposal No. 98G110).

References

[1] Y. Iwasawa, in: R.W. Joyner, R.A. van Santen (Eds.), Elementary Reaction Steps in Heterogeneous Catalysis, NATO ASI Series C, Vol. 398, 1993, p. 287.

[2] Y. Iwasawa, Acc. Chem. Res. 30 (1997) 103.
[3] Y. Iwasawa, in: Abstracts of the 7th Japan–China–USA Symposium on Catalysis, Tokyo, 1995, p. 49.
[4] A. Yamaguchi, K. Asakura, Y. Iwasawa, J. Mol. Catal. A: Chem. 146 (1999) 65.
[5] A. Yamaguchi, T. Shido, K. Asakura, Y. Iwasawa, in: Proceedings of 12th International Congress on Catalysis, 2000, in press.
[6] Y. Iwasawa, K. Asakura, H. Ishii, H. Kuroda, Z. Phys. Chem. N.F. 144 (1985) 105.
[7] Y. Iwasawa, Adv. Catal. 35 (1987) 187.
[8] M. Nishimura, K. Asakura, Y. Iwasawa, J. Chem. Soc., Chem. Commun. (1986) 1660.
[9] T. Ushikubo, et al. (Mitubishi Kasei Corp.), Jpn. Tokkai, H5-208136 H6-116225.
[10] R.H.H. Smits, K. Seshan, J.R.H. Ross, ACS Preprints Petroleum Division 37 (1992) 1121.
[11] T. Ushikubo, Y. Hara, K. Wada, Catal. Today 16 (1993) 525.
[12] M. Nishimura, K. Asakura, Y. Iwasawa, in: Proceedings of the 9th Intrenational Congress on Catalysis, Calgary, Vol. 4, 1988, p. 1566.
[13] T. Shido, K. Asakura, Y. Iwasawa, J. Catal. 122 (1990) 55.
[14] T. Shido, Y. Iwasawa, J. Catal. 129 (1991) 343.
[15] T. Shido, Y. Iwasawa, J. Catal. 136 (1992) 493.
[16] T. Shido, Y. Iwasawa, J. Catal. 140 (1993) 575.
[17] T. Shido, Y. Iwasawa, J. Catal. 141 (1993) 71.
[18] Y. Iwasawa, in: Proceedings of the 11th International Congress on Catalysis, Baltimore, Stud. Surf. Sci. Catal., Vol. 101 Elsevier, Amsterdam, 1996, p. 21.
[19] T. Shido, K. Asakura, Y. Iwasawa, J. Chem. Soc., Faraday Trans. 1 85 (1989) 441.
[20] J. Wei, Adv. Catal 24 (1975) 57.
[21] Y. Iwasawa, M. Yamada, Y. Sato, H. Kuroda, J. Mol. Catal. 23 (1984) 95.
[22] Y. Iwasawa, Supported catalysts from chemical vapor deposition and related techniques, in: G. Ertl, H. Knözinger, J. Weitkamp (Eds.), Handbook of Heterogeneous Catalysis, Vol. 2, Wiley, 1997, p. 853.
[23] P.S. Braterman, Metal Carbonyl Spectra, Academic Press, New York, 1975, p. 43.
[24] K. Asakura, Y. Iwasawa, J. Phys. Chem. 93 (1989) 4213.
[25] T. Shido, A. Yamaguchi, Y. Iwasawa, in press.